Estimating the genome-wide contribution of selection to temporal allele frequency change

Vince Buffalo[a,b,c,1] **and Graham Coop**[b,c]

[a]Population Biology Graduate Group, University of California, Davis, 95616; [b]Center for Population Biology, Department of Evolution and Ecology, University of California, Davis, CA 95616

Rapid phenotypic adaptation is often observed in natural populations and selection experiments. However, detecting the genome-wide impact of this selection is difficult, since adaptation often proceeds from standing variation and selection on polygenic traits, both of which may leave faint genomic signals indistinguishable from a noisy background of genetic drift. One promising signal comes from the genome-wide covariance between allele frequency changes observable from temporal genomic data, e.g. evolve-and-resequence studies. These temporal covariances reflect how heritable fitness variation in the population leads changes in allele frequencies at one timepoint to be predictive of the changes at later timepoints, as alleles are indirectly selected due to remaining associations with selected alleles. Since genetic drift does not lead to temporal covariance, we can use these covariances to estimate what fraction of the variation in allele frequency change through time is driven by linked selection. Here, we reanalyze three selection experiments to quantify the effects of linked selection over short timescales using covariance among time-points and across replicates. We estimate that at least 17% to 37% of allele frequency change is driven by selection in these experiments. Against this background of positive genome-wide temporal covariances we also identify signals of negative temporal covariance corresponding to reversals in the direction of selection for a reasonable proportion of loci over the time course of a selection experiment. Overall, we find that in the three studies we analyzed, linked selection has a large impact on short-term allele frequency dynamics that is readily distinguishable from genetic drift.

Linked Selection | Adaptation | Experimental Evolution

A long-standing problem in evolutionary genetics is quantifying the roles of genetic drift and selection in shaping genome-wide allele frequency changes. Selection can affect allele frequencies, both directly and indirectly, with the indirect effect coming from the action of selection on correlated loci elsewhere in genome, e.g. linked selection (1–3); see (4) for a review. Previous work has mostly focused on teasing apart the impacts of drift and selection on genome-wide diversity using population samples from a single contemporary timepoint, often by modeling the correlation between regional recombination rate, gene density, and diversity created in the presence of linked selection (5, 6). This approach has shown linked selection has a major role in shaping patterns of genome-wide diversity across the genomes of a range of sexual species (7–15), and has allowed us to quantify the relative influence of positive selection (hitchhiking) and negative selection (background selection; (7, 8, 15–18)). However, we lack an understanding of both how linked selection acts over short time intervals and of its full impact on genome-wide allele frequency changes.

There are numerous examples of rapid phenotypic adaptation (19–22) and rapid, selection-driven genomic evolution in asexual populations (23–25). Yet the polygenic nature of fitness makes detecting the impact of selection on genome-wide variation over short timescales in sexual populations remarkably difficult (26–28). This is because the effect of selection on a polygenic trait (such as fitness) is distributed across numerous loci. This can lead to subtle allele frequency shifts on standing variation that are difficult to distinguish from background levels of genetic drift and sampling variance. Increasingly, genomic experimental evolution studies with multiple timepoints, and in some cases multiple replicate populations, are being used to detect large-effect selected loci (29, 30) and differentiate modes of selection (31–33). In addition these temporal-genomic studies have begun in wild populations, some with the goal of finding variants that exhibit frequency changes consistent with fluctuating selection (34, 35). In a previous paper, we proposed that one useful signal for understanding the genome-wide impact of polygenic linked selection detectable from temporal genomic data is the temporal autocovariance (i.e. covariance between two timepoints) of allele frequency changes (36). These covariances are created when the loci that underly heritable fitness variation perturb the frequencies of linked alleles; in contrast, when genetic drift acts alone in a closed population, these covariances are expected to be zero for neutral alleles. Mathematically, temporal covariances are useful because it is natural to decompose the total variance in allele frequency change across a time interval into the variances and covariances in allele frequency change

Significance Statement

A long-standing problem in evolutionary biology is to understand the processes that shape the genetic composition of populations. In a population without migration, the two processes that change allele frequencies are selection, which increases beneficial alleles and removes deleterious ones, and genetic drift which randomly changes frequencies as some parents contribute more or less alleles to the next generation. Previous efforts to disentangle these processes have used genomic samples from a single timepoint and models of how selection affects neighboring sites (linked selection). Here, we use genomic data taken through time to quantify the contributions of selection and drift to genome-wide frequency changes. We show selection acts over short timescales in three evolve-and-resequence studies and has a sizable genome-wide impact.

V.B. and G.C. designed research and wrote paper; V.B. performed research, contributed new reagents/analytic tools, and analyzed data.

The authors declare no conflict of interest.

[1]To whom correspondence should be addressed. E-mail: vsbuffalo@gmail.com

Table 1. Summary of the main selection studies we analyzed

Study	Species	Selection	Replicates	Pop. Size†	Gens.	Timepoints
Kelly and Hughes (2019)	*D. simulans*	lab adaptation	3	∼1100	14	2
Barghi et al. (2019)	*D. simulans*	lab adaptation	10	∼1000	60	7
Castro et al. (2019)	*M. musculus*	tibiae length	2	32	17	2
		control	1	28		

†Approximate census population size during experiment.

between generations. Furthermore, biologically, these covariances reflect the extent to which allele frequency changes in one generation predict changes in another due to a shared selection pressures and associations to selected loci.

Here, we provide the first empirical analyses to quantify the impact of linked selection acting over short timescales (tens of generations) across two evolve and re-sequence studies (32, 37), and an artificial selection experiment (38). These sequencing selection experiments have started to uncover selected loci contributing to the adaptive response; however it is as yet far from clear how much of genome-wide allele frequency changes are driven by selection or genetic drift. We repeatedly find a signal of temporal covariance, consistent with linked selection acting to significantly perturb genome-wide allele frequency changes across the genome in a manner that other approaches would not be able differentiate from genetic drift. We estimate a lower bound of the fraction of variance in allele frequency change caused by selection, as well as the correlation between allele frequency changes between replicate populations caused by convergent selection pressures. Overall, we demonstrate that linked selection has a powerful role in shaping genome-wide allele frequency changes over very short timescales in experimental evolution.

Results

We first analyzed the dataset of Barghi et al. (2019), an evolve-and-resequence study with ten replicate populations exposed to a high temperature lab environment and evolved for 60 generations, and sequenced every ten generations. Using the seven timepoints and ten replicate populations, we estimated the genome-wide 6×6 temporal covariance matrix $\mathbf{Q}$ for each of the ten replicates. Each row of these matrices represent the temporal covariance $\mathrm{Cov}(\Delta_{10} p_s, \Delta_{10} p_t)$, between the allele frequency change (in ten-generation intervals, denoted $\Delta_{10} p_t$) of some initial reference generation s (the row of the matrix), and some later timepoint t (the column of the matrix). We corrected these matrices for biases created due to sampling noise, and normalized the entries for heterozygosity (see SI Appendix, sections S1.2 and S1.4). These covariances are expected to be zero when only drift is acting, as only heritable variation for fitness can create covariance between allele frequency changes in a closed population (36). Averaging across the ten replicate temporal covariances matrices, we find temporal covariances that are statistically significant (95% block bootstraps CIs do not contain zero), consistent with linked selection perturbing genome-wide allele frequency changes over very short time periods. The covariances between all adjacent time intervals are positive and then decay towards zero as we look at more distant time intervals (Figure 1 A), as expected when directional selection affects linked variants' frequency trajectories until ultimately linkage disequilibrium and the associated additive genetic variance for fitness decays (which could occur as a population reaches a new optimum, and directional selection weakens) (36). The temporal covariances per replicate are noisier but this general pattern holds; see SI Appendix, Fig. S23.

Since our covariances are averages over loci, the covariance estimate could be strongly affected by a few outlier regions. To test whether large outlier regions drive the genome-wide signal we see in the Barghi et al. (2019) data, we calculate the covariances in 100kb windows along the genome (we refer to these as windowed covariances throughout) and take the median windowed covariance, and trimmed-mean windowed covariance, as a measure of the genome-wide covariance robust to large-effect loci. These robust estimates (SI Appendix, Table S1 and SI Appendix, Fig. S24) confirm the patterns we see using the mean covariance, establishing that genomic temporal covariances are non-zero due to the impact of selection acting across many genomic regions.

While the presence of positive temporal covariances is consistent with selection affecting allele frequencies over time, this measure is not easily interpretable. We can calculate a more intuitive measure from the temporal covariances to quantify the impact of selection on allele frequency change: the ratio of total covariance in allele frequency change to the total variance in allele frequency change. We denote the change in allele frequency as $\Delta p_t = p_{t+1} - p_t$, where p_t is the allele frequency in generation t. Since the total variation in allele frequency change can be partitioned into variance and covariance components, $\mathrm{Var}(p_t - p_0) = \sum_{i=0}^{t-1} \mathrm{Var}(\Delta p_i) + \sum_{i=0}^{t-1} \sum_{j \neq i}^{t-1} \mathrm{Cov}(\Delta p_i, \Delta p_j)$ (we correct for biases due to sequencing depth), and the covariances are zero when drift acts alone, this is a lower bound on how much of the variance in allele frequency change is caused by linked selection (36). We call this measure $G(t)$, defined as

$$G(t) = \frac{\sum_{i=0}^{t-1} \sum_{j \neq i}^{t-1} \mathrm{Cov}(\Delta p_i, \Delta p_j)}{\mathrm{Var}(p_t - p_0)}. \quad [1]$$

This estimates the impact of selection on allele frequency change between the initial generation 0 and some later generation t, which can be varied to see how this quantity grows through time. When the sum of the covariances is positive, this measure can intuitively be understood as a lower bound on relative fraction of allele frequency change normally thought of as "drift" that is actually due to selection. Additionally, $G(t)$ can be understood as a short-timescale estimate of the reduction in neutral diversity due to linked selection (or equivalently the reduction in neutral effective population size needed to account linked selection, see SI Appendix, section S7). Since the Barghi et al. (2019) experiment is sequenced every ten generations, the numerator uses the covariances estimated between ten-generation blocks of allele

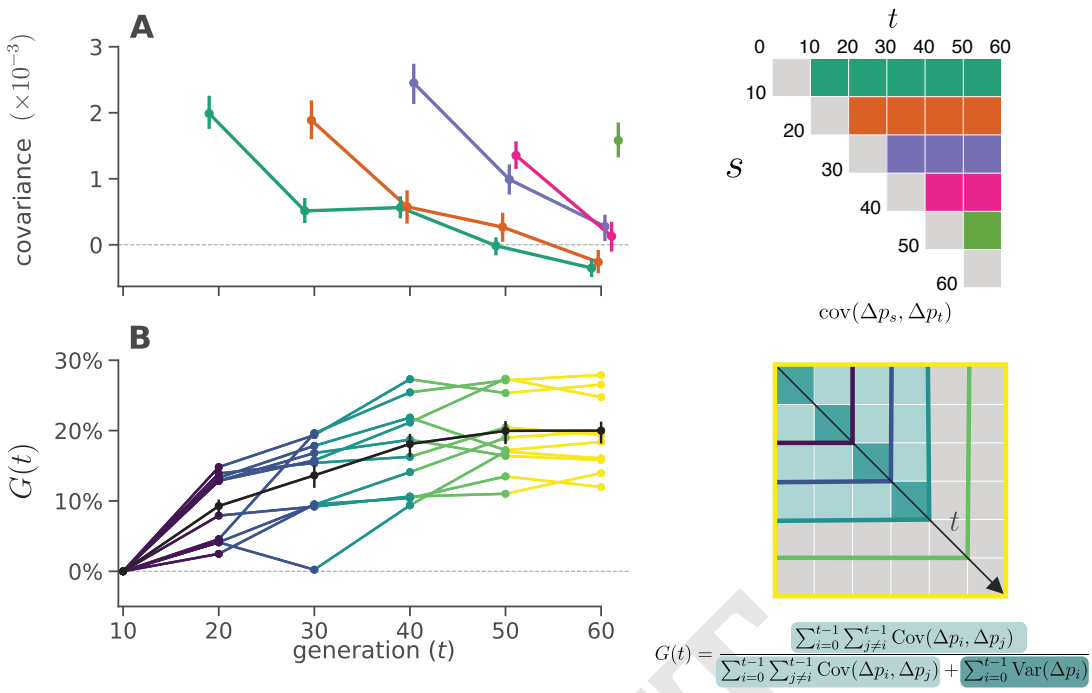

Fig. 1. **A**: Temporal covariance, averaged across all ten replicate populations, through time from the Barghi et al. (2019) study. Each line depicts the temporal covariance $\mathrm{Cov}(\Delta p_s, \Delta p_t)$ from some reference generation s to a later time t which varies along the x-axis; each line corresponds to a row of the upper-triangle of the temporal covariance matrix with the same color (upper right). The ranges around each point are 95% block-bootstrap confidence intervals. **B**: A lower bound on the proportion of the total variance in allele frequency change explained by linked selection, $G(t)$, as it varies through time t along the x-axis. The black line is the $G(t)$ averaged across replicates, with the 95% block-bootstrap confidence interval. The other lines are the $G(t)$ for each individual replicate, with colors indicating what subset of the temporal-covariance matrix to the right is being included in the calculation of $G(t)$.

frequency change; thus the strong, unobservable, covariances between adjacent generations do not contribute to the numerator of $G(t)$. Had these covariances been measurable on shorter timescales, their cumulative effect would likely have been higher yet (see SI Appendix, sections S2 and S8.4 for more details). Additionally, selection inflates the variance in allele frequency change per generation; however, this effect cannot be easily distinguished from drift. For both these reasons, our measure $G(t)$ is quite conservative (we demonstrate this through simulations in SI Appendix, section S8.4). Still, we find a remarkably strong signal. Greater than 20% of total, genome-wide allele frequency change over 60 generations is the result of selection (Figure 1 B). This proportion of variance attributable to selection builds over time in Figure 1B as the effects of linked selection are compounded over the generations unlike genetic drift. Our G(t) starts to plateau to a constant level as the covariances from earlier generations have decayed and so no longer contribute as strongly (Figure 1).

Additionally, we looked for a signal of temporal autocovariance in Bergland et al. (2014), a study that collected *Drosophila melanogaster* through Spring-Fall season pairs across three years. If there was a strong pattern of genome-wide fluctuating selection, we might expect a pattern of positive covariances between similar seasonal changes, e.g. Spring-Fall in two adjacent years, and negative covariances between dissimilar seasonal changes, e.g. Spring-Fall and Fall-Spring in two adjacent years. However, we find no such signal over years, and in reproducing their original analysis, we find that their number of statistically significant seasonal SNPs is not enriched compared to an empirical null distribution created by permuting seasonal labels; we discuss this in more depth in SI Appendix, section S6.

The replicate design of Barghi et al. (2019) allows us to quantify another covariance: the covariance in allele frequency change between replicate populations experiencing convergent selection pressures. These between-replicate covariances are created in the same way as temporal covariances: alleles linked to a particular fitness background are expected to have allele frequency changes in the same direction if the selection pressures are similar. Intuitively, where temporal covariances reflect that alleles associated with heritable fitness backgrounds are predictive of frequency changes between generations, replicate covariances reflect that heritable fitness backgrounds common to each replicate predict (under the same selection pressures) frequency changes between replicates; we note that there is not a direct one-to-one correspondence between temporal and replicate covariances, since the latter are driven by a shared selection pressure and the stochastic genetic backgrounds across replicate populations. We measure this through a statistic similar to a correlation, which we call the convergent correlation: the ratio of average between-replicate covariance across all pairs to the average standard deviation across all pairs of replicates,

$$\mathrm{cor}(\Delta p_s, \Delta p_t) = \frac{\mathbb{E}_{A\neq B}\left(\mathrm{Cov}(\Delta p_{s,A}, \Delta p_{t,B})\right)}{\mathbb{E}_{A\neq B}\left(\sqrt{\mathrm{Var}(\Delta p_{s,A})\,\mathrm{Var}(\Delta p_{t,B})}\right)} \quad [2]$$

where A and B here are two replicate labels, and for the

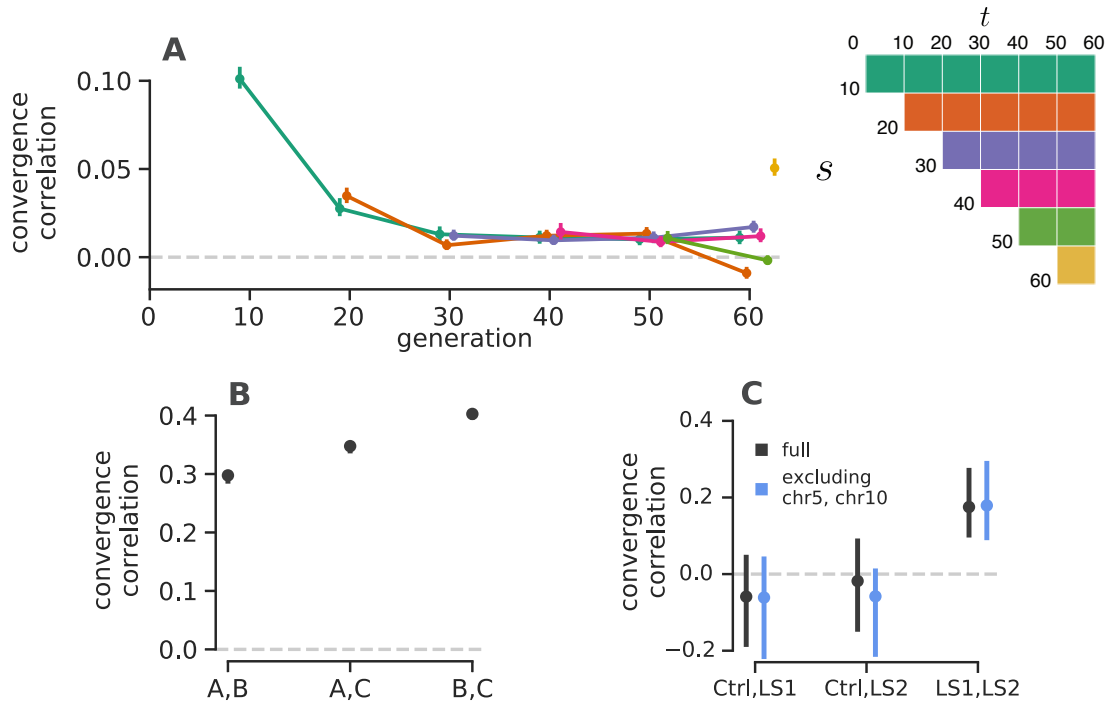

Fig. 2. **A**: The convergence correlations, averaged across Barghi et al. (2019) replicate pairs, through time. Each line represents the convergence correlation $\mathrm{cor}(\Delta p_s, \Delta p_t)$ from a starting reference generation s to a later time t, which varies along the x-axis; each line corresponds to a row of the temporal convergence correlation matrix depicted to the right (where the diagonal elements represent the convergence correlations between the same timepoints across replicate populations). We note that convergent correlation for the last timepoint is an outlier; we are unsure as to the cause of this, e.g. it does not appear to be driven by a single pair of replicates. **B**: The convergence correlations between individual pairs of replicates in the Kelly and Hughes (2019) data (note the confidence intervals are plotted, but are small on this y-axis scale). **C**: The convergence correlations between individual pairs of replicates in (38) data, for the two selection lines (LS1 and LS2) and the control (Ctrl); gray CIs are those using the complete dataset, blue CIs exclude chromosomes 5 and 10 which harbor the two regions Castro et al. (2019) found to have signals of parallel selection between LS1 and LS2. Through simulations, we have found that the differences in convergence correlation confidence interval widths between these *Drosophila* studies and the Longshanks study are due to the differing population sizes.

Barghi et al. (2019) data, we use $\Delta_{10} p_t$.

We have calculated the convergent correlation for all rows of the replicate covariance matrices. Like temporal covariances, we visualize these through time (Figure 2A), with each line representing the convergent correlation from a particular reference generation s as it varies with t (shown on the x-axis). In other words, each of the colored lines corresponds to the like-colored row of the convergence correlation matrix (upper left in Figure 2A). We find these convergent correlation coefficients are relatively weak, and decay very quickly from an initial value of about 0.1 (95% block bootstrap confidence intervals $[0.094, 0.11]$) to around 0.01 (95% CIs $[0.0087, 0.015]$) within 20 generations. This suggests that while a substantial fraction of the initial response is shared over the replicates, this is followed by a rapid decay, a result consistent with the primary finding of the original Barghi et al. (2019) study: that alternative loci contribute to longer term adaptation across the different replicates.

A benefit of between-replicate covariances is that unlike temporal covariances, these can be calculated with only two sequenced timepoints and a replicated study design. This allowed us to assess the impact of linked selection in driving convergent patterns of allele frequency change across replicate populations in two other studies. First, we reanalyzed the selection experiment of Kelly and Hughes (2019), which evolved three replicate wild populations of *Drosophila simulans* for 14 generations adapting to a novel laboratory environment. Since each replicate was exposed to the same selection pressure and share linkage disequilibria common to the original natural founding population, we expected each of the three replicate populations to have positive convergence correlations. We find all three convergent correlation coefficients between replicate pairs are significant (Figure 2B), and average to 0.36 (95% CI $[0.31, 0.40]$). Additionally, we can calculate the proportion of the total variance in allele frequency change from convergent selection pressure, analogous to our $G(t)$, where the numerator is the convergent covariance and the denominator is the total variance (see SI appendix, section S4). We find that 37% of the total variance is due to shared allele frequency changes caused by selection (95% CI [29%, 41%]; these are similar to the convergence correlation, since the variance is relatively constant across the replicates.

Next, we reanalyzed the Longshanks selection experiment, which selected for longer tibiae length relative to body size in mice, leading to a response to selection of about 5 standard deviations over the course of twenty generations (38, 39). This study includes two independent selection lines, Longshanks 1 and 2 (LS1 and LS2), and an unselected control line (Ctrl) where parents were randomly selected. Consequently, this selection experiment offers a useful control to test our convergence correlations: we expect to see significant positive convergence correlations in the comparison between the two Longshanks selection lines, but not between each of the control line and Longshanks line pairs. We find that this is the

case (gray confidence intervals in Figure 2C), with convergence correlations between each of the Longshanks lines to the control not being statistically different from zero, while the convergence correlation between the two Longshanks lines is strong (0.18) and statistically significant (CIs [0.07, 0.25]).

One finding in the Longshanks study was that two major-effect loci showed parallel frequency shifts between the two selection lines. We were curious to what extent our genome-wide covariances were being driven by these two outlier large-effect loci, so we excluded them from the analysis. Since we do not know the extent to which linkage disequilibrium around these large-effect loci affects neighboring loci, we took the conservative precaution of excluding the entire chromosomes these loci reside on (chromosomes 5 and 10), and re-calculating the temporal covariances. We find excluding these large effect loci has little impact on the confidence intervals (blue confidence intervals in Figure 2C), indicating that these across-replicate covariances are indeed driven by a large number of loci. This is consistent with a signal of selection on a polygenic trait driving genome-wide change, although we note that large-effect loci can contribute to the indirect change at unlinked loci (40, 41).

The presence of an unselected control line provides an alternative way to partition the effects of linked selection and genetic drift: we can compare the total variance in allele frequency change of the control line (which excludes the effect of artificial selection on allele frequencies) to the total variance in frequency change of the Longshanks selection lines. This allows us to estimate the increase in variance in allele frequency change due to selection, which we can further partition into the effects of selection shared between selection lines and those unique to a selection line by estimating the shared effect through the observed covariance between replicates (see Materials and Methods 1 and SI Appendix, section S4 for more details). We estimate at least 32% (95% CI [21%, 48%]) of the variance in allele frequency change is driven by the effects of selection, of which 14% (95% CI [3%, 33%]) is estimated to be unique to a selection line, and 17% (95% CI [9%, 23%]) is the effect of shared selection between the two Longshanks selection lines.

We observed that in the longest study we analyzed (32), some genome-wide temporal covariances become negative at future timepoints (see the first two rows in Figure 1A). This shows that alleles that were on average going up initially are later going down in frequency, i.e. that the average direction of selection experienced by alleles has flipped. This might reflect either a change in the environment or the genetic background, due to epistatic relationships among alleles altered by frequency changes (which can occur during an optima shift; (42)) or recombination breaking up selective alleles. Such reversals in selection dynamics could be occurring at other timepoints but the signal of a change in the direction of selection at particular loci may be washed out when we calculate our genome-wide average temporal covariances. To address this limitation, we calculated the distribution of the temporal covariances over 100kb windowed covariances (Figure 3 shows these distributions pooling across all replicates; see SI Appendix, Fig. S26 for individuals replicates). The covariance estimate of each genomic window will be noisy, due to sampling and genetic drift, and the neutral distribution of the covariance is complicated due to linkage disequilibria,

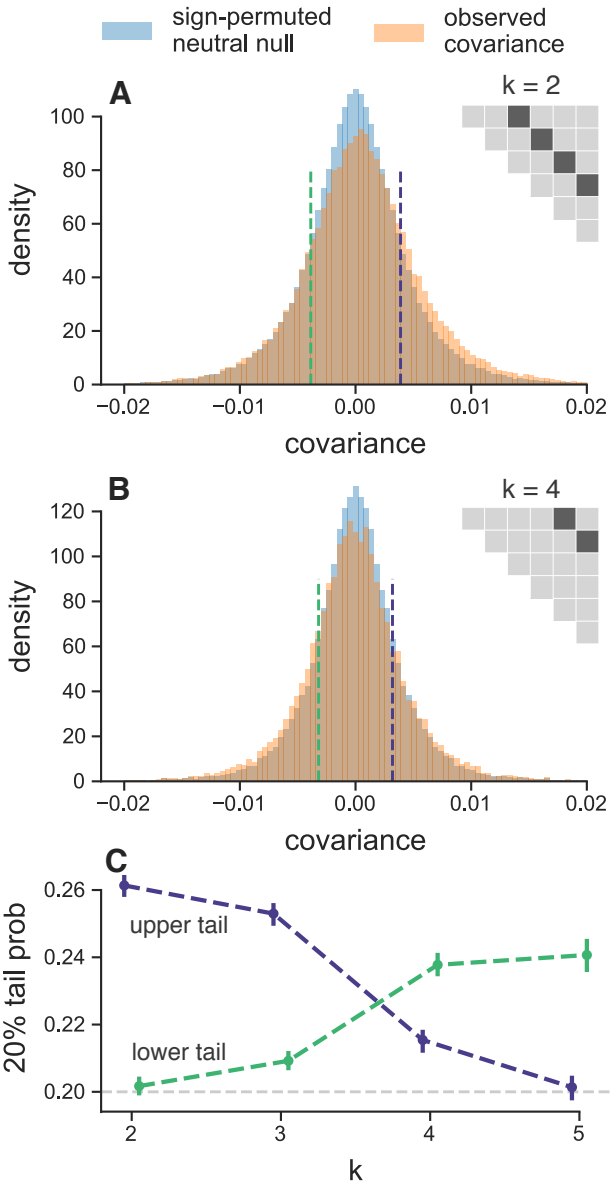

Fig. 3. **A**, **B**: The distribution of temporal covariances calculated in 100kb genomic windows from the Barghi et al. (2019) study, plotted alongside an empirical neutral null distribution created by recalculating the windowed covariances on 1,000 sign permutations of allele frequency changes within tiles. The number of histogram bins is 88, chosen by cross validation (SI Appendix, section S25). In subfigure **A**, windowed covariances $\mathrm{Cov}(\Delta p_t, \Delta p_{t+k})$ are separated by $k = 2 \times 10$ generations and in subfigure **A** the covariances are separated by $k = 4 \times 10$ generations; each k is an off-diagonal from the variance diagonal of the temporal covariance matrix (see cartoon of upper-triangle of covariance matrix in subfigures **A** and **B**, where the first diagonal is the variance, and the dark gray indicates which off-diagonal of the covariance matrix is plotted in the histograms). **C**: The lower and upper tail probabilities of the observed windowed covariances, at 20% and 80% quintiles of the empirical neutral null distribution, for varying time between allele frequency changes (i.e. which off-diagonal k). The confidence intervals are 95% block-bootstrap confidence intervals, and the light gray dashed line indicates the 20% tail probability expected under the neutral null. Similar figures for different values of k are in SI Appendix, section S27.

which can occur over long physical distances in E&R and selection studies (43, 44). To address this, we have developed a permutation-based procedure that constructs an empirical neutral null distribution by randomly flipping the sign of the allele frequency changes in each genomic window (i.e. a single random sign flip is applied to all loci in a window). This destroys the systematic covariances created by linked selection and creates a sampling distribution of the covariances spuriously created by neutral genetic drift while preserving the complex dependencies between adjacent loci created by linkage disequilibrium. This empirical neutral null distribution is conservative in the sense that the variances of the covariances are wider than expected under drift alone, as selection not only creates covariance between time intervals, but also inflates the magnitude of allele frequency change within a time-interval. We see (Figure 3 A and B) that there are an empirical excess of windows with positive covariances between close timepoints compared to the null distribution (a heavier right tail), and that this then shifts to an excess of windows with negative covariances between more distant timepoints (a heavier left tail).

We quantified the degree to which the left and right tails are inflated compared to the null distribution as a function of time, and see excesses in both tails in Figure 3C. This finding is also robust to sign-permuting allele frequency changes on a chromosome-level, the longest extent that gametic linkage disequilibria can extend (SI Appendix, Fig. S29). We see a striking pattern that the windowed covariances not only decay towards zero, but in fact become negative through time, consistent with many regions in the genome having had a reversed fitness effect at later timepoints.

Finally we used forward-in-time simulations to explore the conditions under which temporal and convergent correlations arise. We show a subset of our results for a model of stabilizing selection on a phenotype where directional selection is induced by a sudden shift in the optimum phenotype of varying magnitudes (Figure 4A). We find that positive temporal covariances are produced by such selection (Figure 4B), and that these positive temporal covariances can compound together to generate a large proportion of allele frequency change being due to selection (i.e. large $G(t)$) over the relatively short time periods similar to our analyzed selection datasets span (Figure 4C). The magnitude of $G(t)$ increases with the strength of selection, i.e. the variance in fitness, such that stronger selection generates larger proportions of allele frequency change. We find a similar picture of stronger convergent selection pressures generating larger convergence correlations (Figure 4D; see also SI Appendix, Fig. S12 for how other factors impact convergence correlations).

Averaging across replicates, these simulation results show $G(t)$ is relatively insensitive to the number of loci underlying the trait. However, if only a small number of loci influence the trait, the $G(t)$ trajectories are typically much more stochastic *across* replicates. This reaffirms that the genome-wide linked selection response we see in the Barghi et al. (2019) data is highly polygenic (compare Figure 1B to SI Appendix, Fig. S6). Furthermore, using our simulations we find that sampling only every 10 generations does indeed mean that our estimates of $G(t)$ are an underestimate of the proportional effect of linked selection as they cannot include the covariance between closely spaced generations (see SI Appendix, Fig. S14).

Additionally, we explored other modes of selection with simulations. We find that the long term dynamics of the covariances under directional truncation selection, which generates substantial epistasis, are richer than we see under Gaussian Stabilizing Selection (GSS) and multiplicative selection (SI Appendix, Fig. S18). We also conducted simulations of purifying selection alone (i.e. background selection) and find that this can also generate positive temporal covariances (SI Appendix, Fig. S16) and under some circumstances, can even generate convergence correlations (SI Appendix, Fig. S17). Thus it is unlikely that the signatures of linked selection we see are entirely the result of the novel selection pressure the populations are exposed to, and some of this signature may be ongoing purifying selection. Only in the case of the Longshanks experiment, does the control line allow us to conclude that selection that is almost entirely due to the novel selection pressure.

While none of our experiments have selected the populations in divergent directions, in our simulations we find that such selection can generate negative convergent correlations (Figure 4D). This suggests that selection experiments combining multiple replicates, control lines, as well as divergent selection pressures might be quite informative in disentangling the contribution of particular selection pressures from genome-wide allele frequency changes.

Discussion

Since the seminal analysis of Maynard Smith and Haig (1974) demonstrating that linked neutral diversity is reduced as an advantageous polymorphism sweeps to fixation, over four decades of theoretical and empirical research has bettered our understanding of linked selection. One under-used approach to understand the genome-wide effects of selection on polygenic trait (e.g. on standing variation, stems from an early quantitative genetic model of linked selection (40) and its later developments (41, 45–47); see also (4) for a comparison of these models with classic hitchhiking models). Implicit in these models is that autocovariance between allele frequency change is created when there is heritable fitness variation in the population, a signal that may be readily detected from temporal genomic data (36). Depending on how many loci affect fitness, even a strong effect of linked selection may not be differentiable from genetic drift using only single contemporary population samples or looking at temporal allele frequency change at each locus in isolation. In this way, averaging summaries of temporal data allows us to sidestep the key problem of detecting selection from standing variation: that the genomic footprint leaves too soft of a signature to differentiate from a background of genetic drift. In fact we find that the temporal covariance signal is detectable even in the extremely difficult to detect case of selection on highly polygenic traits (36).

It is worth building some intuition why temporal covariance allows us to detect such faint signals of polygenic linked selection from temporal genomic data. Variance in allele frequency change is subject to both drift and sampling noise, which at any single locus may swamp the temporal covariance signal due to selection, or create spurious covariances when selection is not acting. However, these spurious covariances do not share a directional signal whereas the covariances cre-

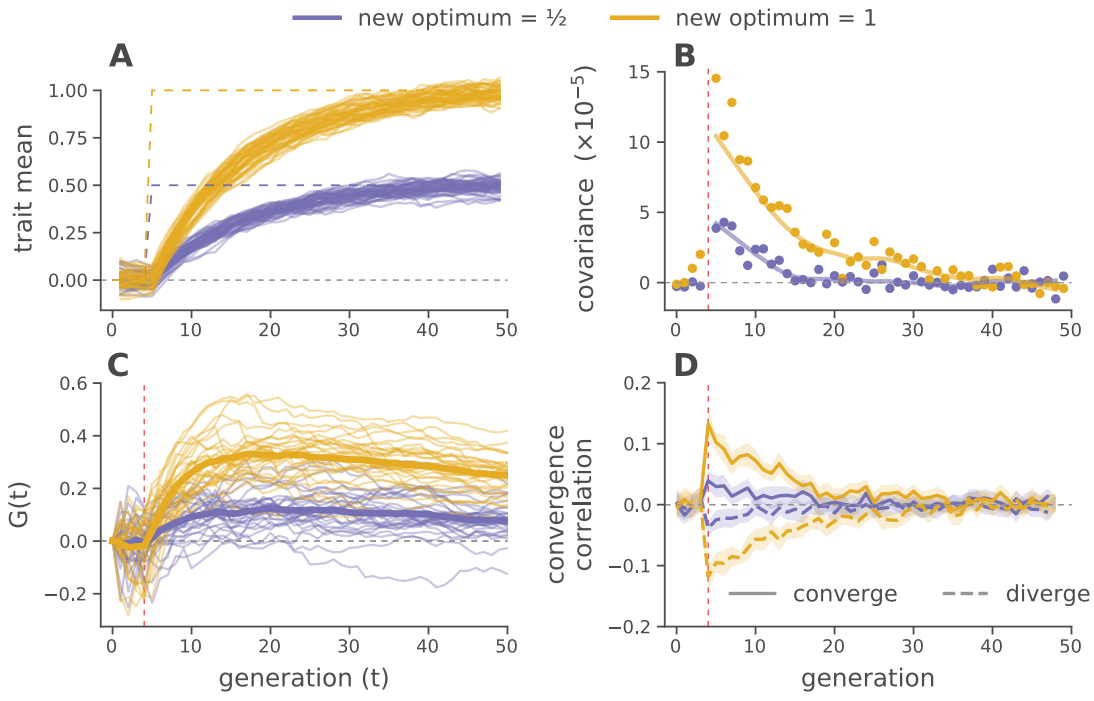

Fig. 4. Forward-in-time simulations demonstrate how temporal covariance, $G(t)$ trajectories, and convergence correlations arise during optima shifts of two different magnitudes, under Gaussian stabilizing selection. ($\mathbf{A}$) Trait means across 30 replicate before and after optima shifts (solid lines), for two different magnitudes (indicated by color). The optimal trait values are indicated by the purple and yellow dashed lines. ($\mathbf{B}$) Mean temporal covariance $\mathrm{Cov}(\Delta p_5, \Delta p_t)$ across 30 simulation replicates, where t varies along the x-axis (points), with a loess-smoothed average (solid line). ($\mathbf{C}$) $G(t)$ trajectories through time, for 30 replicate simulations across two optima shifts. The solid line is a loess-smoothed average. ($\mathbf{D}$) The convergence correlations between two populations (each 1000 diploids) split from a common population, that underwent either an optima shift in the same direction (converge) and opposite directions (diverge) at generation five. In subfigures ($\mathbf{B}$), ($\mathbf{C}$), and ($\mathbf{D}$), directional selection begins at generation five, when the optima shifts; this is indicated by the vertical dashed red line (see SI Appendix Section S8.2 for details on these simulations).

ated by linked selection do; consequently, averaging across the entire genome, the temporal signal exceeds sampling noise.

Our analyses reveal that a sizable proportion of allele frequency change in these experimental evolution populations is due to the (likely indirect) action of selection. Capitalizing on replicated designs, we characterized the extent to which convergent selection pressures lead to parallel changes in allele frequencies across replicate populations, and found that a substantial proportion of the response is shared across short timescales. These likely represent substantial under-estimates of the contribution of linked selection because the studies we have reanalyzed do not sequence the population each generation, preventing us from including the effects of stronger correlations between adjacent generations. Furthermore, our estimation methods are intentionally conservative, for example they exclude the contribution of selection that does not persist across generations and selection that reverses sign; thus they can be seen as a lower bound of the effects of selection, which we have confirmed through forward-in-time simulations. Finally, through simulation results, we show that for a given level of additive genetic variance, the strengths of temporal and replicate covariances depend on the mode of selection, the details of the populations or selection experiment, and the level of linkage disequilibria, yet the level of temporal covariance is relatively invariant to the number of loci underlying fitness, as long as fitness is sufficiently polygenic.

These estimates of the contribution of selection could be refined by using patterns of linkage disequilibria (LD) and recombination which would allow us to more fully parameterize a linked-selection model of temporal allele frequency change (36). The basic prediction is that regions of higher linkage disequilibrium and lower recombination should have greater temporal autocovariance than regions with lower LD and higher recombination. However, one limitation of these pooled sequence datasets is that none of the studies we reanalyzed estimated linkage disequilibria data for the evolved populations. While there are LD data for a natural population of *D. simulans* (48, 49), we did not find a relationship between temporal covariance and LD. We believe this is driven by the idiosyncratic nature of LD in evolve-and-resequence populations, which often extends over large genomic distances (37, 43). Future studies complete with LD data and recombination maps would allow one to disentangle the influence of closely linked sites from more distant sites in causing temporal autocovariance, and allow the fitting of more parametric models to estimate population parameters such as the additive genetic variance for fitness directly from temporal genomic data alone (36). Future work could refine our $G(t)$ estimates by including selection's impact on the variance in allele frequency terms (e.g. see equation 26 of (36)), and possibly quantifying the covariances missed when sequencing is not done each generation; both would lead to less conservative estimates that could show a large impact of selection.

Our primary focus here has been on evolution in laboratory populations. It is unclear whether we should expect a similar impact of selection in natural populations. In some of these experiments, selection pressures may have been stronger or more sustained than in natural populations (50, 51). Conversely, these lab populations were maintained at relatively small census sizes (Table 1), which will amplify the role of genetic drift, and increase the frequency of rare deleterious alleles in selection lines due to founder effects. The advantage of lab experiments is that they are closed populations; in natural populations temporal covariance could also arise from the systematic migration of alleles from differentiated populations. Adapting these methods to natural populations will require either populations that are reasonably closed to migration, or for the effect of migration to be accounted for possibly either by knowledge of allele frequencies in source populations or the identification of migrant individuals.

While it challenging to apply temporal methods to natural populations there is a lot of promise for these approaches (34, 35). Efforts to quantify the impact of linked selection have found obligately sexual organisms have up to an 89% reduction in genome-wide diversity over long time periods (15, 17, 52–54) Thus linked selection makes a sizeable contribution to long-term allele frequency change in some species, and there is reason to be hopeful that we could detect this from temporal data, which would help to resolve the timescales that linked selection acts over in the wild. In our reanalysis of the Barghi et al. (2019) study, we find evidence of complex linked selection dynamics, with selection pressures flipping over time due to either environmental change, the breakup of epistatic combinations or advantageous haplotypes. Such patterns would be completely obscured in samples from only contemporary populations. Thus, we can hope to have a much richer picture of the impact of selection as temporal sequencing becomes more common, allowing us to observe the effects of ecological dynamics in genomic data (51).

Furthermore, understanding the dynamics of linked selection over short timescales will help to unite phenotypic studies of rapid adaptation with a detectable genomic signature, to address long-standing questions concerning linked selection, evolutionary quantitative genetics, and the overall impact selection has on genetic variation.

Materials and Methods

Datasets Analyzed. We used available genomic data data from four studies: pooled population resequencing (pool-Seq) data from Barghi et al. (2019), Kelly and Hughes (2019), and Bergland et al. (2014), and individual-level sequencing data from Castro et al. (2019). In all cases, we used the variants kept after the filtering criteria of the original studies.

Variance and Covariance Estimates. To remove systematic covariances in allele frequency change caused by tracking the reference or minor allele, we randomly choose an allele to track frequency for each locus. Then, we calculate the variance-covariance matrix of allele frequency changes using a Python software package we have written, available at http://github.com/vsbuffalo/cvtk. This simultaneously calculates temporal variances and covariances, and replicate covariances and uses the sampling depth and number of diploid individuals to correct for bias in the variance estimates and a bias that occurs in covariance estimates between adjacent timepoints due to shared sampling noise (see SI Appendix, sections S1.2, S1.3, and S1.4 for mathematical details of these estimators). We assess that our bias correction procedure is working adequately through a series of diagnostic plots that ensure that the procedure removes the relationship between sampling depth and uncorrected variance and covariances (SI Appendix, Fig. S4). Through our simulations we find that our estimates can differ based on how fixations and losses are handled in long time-series (SI Appendix, section S8.7) but none of our findings in the main text are qualitatively altered by this decision (SI Appendix, Figs. S19 and S20).

Estimating Uncertainty with a Block Bootstrap. To infer the uncertainty of covariance, convergence correlation, and $G(t)$ estimates, we used a block bootstrap procedure. This bootstrap procedure resamples blocks of loci, rather than individual loci, to infer the uncertainty of a statistic in the presence of unknown correlation between loci. As most estimators in this paper are ratios (e.g. covariance standardize by sample heterozygosity, $G(t)$, and the convergence correlation), which we estimate with a ratio of averages, we exploit the linearity of expectation for efficient computation of bootstrap samples (see SI Appendix, Fig. S3 for details).

Partitioning Unique and Shared Selection Effects in the Longshanks Study. The unselected control line in the Longshanks experiment allows us to additionally partition the total variance in allele frequency change into drift, shared effects of selection, and unshared effects of selection between selected replicates. We begin by decomposing the allele frequency change in Longshanks line 1 (LS1) as $\Delta p_{t,\mathrm{LS1}} = \Delta_D p_{t,\mathrm{LS1}} + \Delta_U p_{t,\mathrm{LS1}} + \Delta_S p_{t,\mathrm{LS}}$ where these terms are the drift in Longshanks replicate 1 ($\Delta_D p_{t,\mathrm{LS1}}$), selection unique to the LS1 replicate ($\Delta_U p_{t,\mathrm{LS1}}$), and selection response shared between the two Longshanks replicates ($\Delta_S p_{t,\mathrm{LS}}$) respectively (and similarly for the Longshanks line 2, LS2). By construction, this decomposition assumes that each of these terms are uncorrelated within replicates, so the contribution of each term to the total variance in allele frequency change, $\mathrm{Var}(\Delta p_{t,\mathrm{LS1}})$, is the variance of that term's allele frequency change.

We estimate the effects of selection by first calculating the fraction of the total variance explained by drift. We assume the variance in allele frequency change observed in the unselected control line ($\mathrm{Var}(\Delta p_{t,\mathrm{Ctrl}})$) is driven entirely by neutral genetic drift, and since an identical breeding scheme was used across all three replicates (except breeders for the control line were chosen at random), we can use this as an estimate of the contribution of neutral genetic drift in the selected lines, $\mathrm{Var}(\Delta p_{t,\mathrm{Ctrl}}) = \mathrm{Var}(\Delta_D p_{t,\mathrm{LS1}}) = \mathrm{Var}(\Delta_D p_{t,\mathrm{LS2}})$. Then, we can estimate the increase in variance in allele frequency change due to selection as $(\mathrm{Var}(\Delta p_{t,\mathrm{LS1}}) + \mathrm{Var}(\Delta p_{t,\mathrm{LS2}}))/2 - \mathrm{Var}(\Delta p_{t,\mathrm{Ctrl}})$ and the shared effect of selection across selected lines as $\mathrm{Cov}(\Delta p_{t,\mathrm{LS1}}, \Delta p_{t,\mathrm{LS2}})$. Finally, the covariance in allele change between replicates is used to estimate the shared effects of selection between lines, $\mathrm{Cov}(\Delta p_{t,\mathrm{LS1}}, \Delta p_{t,\mathrm{LS2}}) = \mathrm{Var}(\Delta_S p_{t,\mathrm{LS}})$.

Windowed Covariance and the Empirical Neutral Null. Throughout the paper, we use genomic windows for the block-bootstrap procedure. For the *D. simulans* and *D. melanogaster* data from the Barghi et al. (2019), Kelly and Hughes (2019), and Bergland et al. (2014) studies, we used large megabase windows for the block bootstrap procedure, while we used a ten megabase window for the large mouse genome data from the Castro et al. (2019) study.

Given evidence of a reversal in the direction of selection at later timepoints in the Barghi et al. (2019) study, we calculated windowed temporal covariances on 10 kilobase windows and looked at the distribution of these covariances through time. We compare these distributions of windowed covariances to an empirical neutral null created by randomly permuting the sign of allele frequency change at the block level (to preserve the correlation structure between loci due to LD). This destroys the systematic covariances in allele frequency change created by linked selection, which emulates a frequency trajectory under drift. This approach is conservative, since heritable fitness variation also inflates the magnitude of allele frequency change more than expected under drift, but we do not change these magnitudes. Using this empirical neutral null distribution of windowed covariances, we calculate how much of the observed windowed covariance distribution falls outside of empirical null distribution for different tail probabilities. While the comparison between the distribution of 10 kilobase windowed covariances to the empirical neutral null created from sign-permuting 10 kilobase windows is most natural, we wanted to ensure that our finding that the shift from mostly positive to mostly negative windowed covariances through time (Figure 3) was robust to LD extending beyond the range of these 10 kilobase windows. We took the conservative approach of also sign-permuting at the chromosome-level, and found the same qualitative shift (SI Appendix, Fig. S29).

Forward-in-time Simulations. To explore how aspects of genetic architecture, models of selection, and experimental design impact temporal covariance, the $G(t)$ trajectories, and convergence correlations, we ran extensive forward-in-time simulations using SLiM (55); here we discuss the Gaussian Stabilizing Selection simulations in Figured 4, but SI Appendix, section S8 describes these simulation routines and others in detail.

We simulated directional selection on a trait by first evolving each population of $N = 1000$ diploids to equilibrium (we will refer to this as the burnin hereafter) under GSS for $10N$ generations with the stabilizing selection variance $V_s = 1$ and an optima set at zero. We note that the small burnin population size means that these simulations should not be taken as reflecting any specific natural population and they are for illustrative purposes only. We simulated a polygenic architecture by setting the trait mutation rate to 10^{-8} per basepair, per generation, in addition to having a separate neutral mutation of 10^{-8} which created neutral mutations which we used to calculate the temporal covariances. Our simulated region was 50 megabases in length (about one quarter of a *Drosophila* chromosome), and trait alleles were randomly selected to have a ± 0.01 effect size. By tracking the trait mean through the burnin, we found it converged to the optimum as expected. After the burnin, the population was split into two different replicate populations, to capture the effect of bottlenecks in selection experiments (these population sizes varied between 50, 500, and 1000 diploids; the later representing no bottleneck). Each population then underwent an optima shift of either 0.1, 0.5, or 1 on generation five, with the first four generations serving as a control. These optima shifts were either in the same direction (converging), different directions (diverging), or only one optima shifted (as a control). By tracking the trait mean, we saw that it converged as expected during burnin, and the trait showed the expected directional response to selection (SI Appendix, Fig. S7). Using the neutral population frequency data from these simulations, we calculated the temporal covariances, $G(t)$ trajectories, and convergence correlations.

Data Availability. All analysis was done in Python, using numpy, matplotlib, and Jupyter notebooks (56–59); code to reproduce these analyses is available on Github, https://github.com/vsbuffalo/cvtk/. All data is from previous studies and available; Barghi et al. (2019) data was downloaded from https://datadryad.org/resource/doi:10.5061/dryad.rr137kn, Kelly and Hughes (2019) data was downloaded from https://gsajournals.figshare.com/articles/Supplemental_Material_for_Kelly_and_Hughes_2018/7124963, Bergland et al. (2014) data was downloaded from https://datadryad.org/stash/dataset/doi:10.5061/dryad.v883p, and Castro et al. (2019) data was downloaded from http://ftp.tuebingen.mpg.de/fml/ag-chan/Longshanks/.

ACKNOWLEDGMENTS. We would like to thank the authors of the original studies we have analyzed, including Neda Barghi, Nick Barton, Alan Bergland, Frank Chan, Kimberly Hughes, John Kelly, Dmitri Petrov, Campbell Rolian, Christian Schlötterer. We would also like to thank Doc Edge for helpful statistical advice, and Dave Begun, Erin Calfee, Sarah Friedman, Andy Kern, Chuck Langley, Michael Turelli, Matt Osmond, Peter Ralph, and Sivan Yair for helpful discussions. Additionally, we thank Guy Sella and an anonymous reviewer whose comments greatly improved the manuscript. This research was supported by an NSF Graduate Research Fellowship grant awarded to VB (1650042), and NIH (R01-GM108779) and NSF (1353380) awarded to GC.

Acknowledgments

1. Maynard Smith J, Haigh J (1974) The hitch-hiking effect of a favourable gene. *Genet. Res.* 23(1):23–35.
2. Charlesworth B, Morgan MT, Charlesworth D (1993) The effect of deleterious mutations on neutral molecular variation. *Genetics* 134(4):1289–1303.
3. Nordborg M, Charlesworth B, Charlesworth D (1996) The effect of recombination on background selection*. *Genet. Res.* 67(02):159–174.
4. Barton NH (2000) Genetic hitchhiking. *Philos. Trans. R. Soc. Lond. B Biol. Sci.* 355(1403):1553–1562.

5. Cutter AD, Payseur BA (2013) Genomic signatures of selection at linked sites: unifying the disparity among species. *Nat. Rev. Genet.* 14(4):262–274.
6. Sella G, Petrov DA, Przeworski M, Andolfatto P (2009) Pervasive natural selection in the drosophila genome? *PLoS Genet.* 5(6):e1000495.
7. Macpherson JM, Sella G, Davis JC, Petrov DA (2007) Genomewide spatial correspondence between nonsynonymous divergence and neutral polymorphism reveals extensive adaptation in drosophila. *Genetics* 177(4):2083–2099.
8. Andolfatto P (2007) Hitchhiking effects of recurrent beneficial amino acid substitutions in the drosophila melanogaster genome. *Genome Res.* 17(12):1755–1762.
9. Begun DJ, et al. (2007) Population genomics: whole-genome analysis of polymorphism and divergence in drosophila simulans. *PLoS Biol.* 5(11):e310.
10. Beissinger TM, et al. (2016) Recent demography drives changes in linked selection across the maize genome. *Nat Plants* 2:16084.
11. Sattath S, Elyashiv E, Kolodny O, Rinott Y, Sella G (2011) Pervasive adaptive protein evolution apparent in diversity patterns around amino acid substitutions in drosophila simulans. *PLoS Genet.* 7(2):e1001302.
12. Williamson RJ, et al. (2014) Evidence for widespread positive and negative selection in coding and conserved noncoding regions of capsella grandiflora. *PLoS Genet.* 10(9):e1004622.
13. Andersen EC, et al. (2012) Chromosome-scale selective sweeps shape caenorhabditis elegans genomic diversity. *Nat. Genet.* 44(3):285–290.
14. Cutter AD, Choi JY (2010) Natural selection shapes nucleotide polymorphism across the genome of the nematode caenorhabditis briggsae. *Genome Res.* 20(8):1103–1111.
15. Elyashiv E, et al. (2016) A genomic map of the effects of linked selection in drosophila. *PLoS Genet.* 12(8):e1006130.
16. Nordborg M, et al. (2005) The pattern of polymorphism in arabidopsis thaliana. *PLoS Biol.* 3(7):e196.
17. McVicker G, Gordon D, Davis C, Green P (2009) Widespread genomic signatures of natural selection in hominid evolution. *PLoS Genet.* 5(5):e1000471.
18. Hernandez RD, et al. (2011) Classic selective sweeps were rare in recent human evolution. *Science* 331(6019):920–924.
19. Grant PR, Grant BR (2011) Causes of lifetime fitness of darwin's finches in a fluctuating environment. *Proc. Natl. Acad. Sci. U. S. A.* 108(2):674–679.
20. Grant PR, Grant BR (2006) Evolution of character displacement in darwin's finches. *Science* 313(5784):224–226.
21. Reznick DN, Shaw FH, Rodd FH, Shaw RG (1997) Evaluation of the rate of evolution in natural populations of guppies (poecilia reticulata). *Science* 275(5308):1934–1937.
22. Franks SJ, Sim S, Weis AE (2007) Rapid evolution of flowering time by an annual plant in response to a climate fluctuation. *Proc. Natl. Acad. Sci. U. S. A.* 104(4):1278–1282.
23. Good BH, McDonald MJ, Barrick JE, Lenski RE, Desai MM (2017) The dynamics of molecular evolution over 60,000 generations. *Nature* 551(7678):45–50.
24. Bennett AF, Dao KM, Lenski RE (1990) Rapid evolution in response to high-temperature selection. *Nature* 346(6279):79–81.
25. Baym M, et al. (2016) Spatiotemporal microbial evolution on antibiotic landscapes. *Science* 353(6304):1147–1151.
26. Latta RG (1998) Differentiation of allelic frequencies at quantitative trait loci affecting locally adaptive traits. *Am. Nat.* 151(3):283–292.
27. Pritchard JK, Pickrell JK, Coop G (2010) The genetics of human adaptation: hard sweeps, soft sweeps, and polygenic adaptation. *Curr. Biol.* 20(4):R208–15.
28. Kemper KE, Saxton SJ, Bolormaa S, Hayes BJ, Goddard ME (2014) Selection for complex traits leaves little or no classic signatures of selection. *BMC Genomics* 15(1):246.
29. Turner TL, Stewart AD, Fields AT, Rice WR, Tarone AM (2011) Population-based resequencing of experimentally evolved populations reveals the genetic basis of body size variation in drosophila melanogaster. *PLoS Genet.* 7(3):e1001336.
30. Turner TL, Miller PM (2012) Investigating natural variation in drosophila courtship song by the evolve and resequence approach. *Genetics* 191(2):633–642.
31. Burke MK, et al. (2010) Genome-wide analysis of a long-term evolution experiment with drosophila. *Nature* 467(7315):587–590.
32. Barghi N, et al. (2019) Genetic redundancy fuels polygenic adaptation in drosophila. *PLoS Biol.* 17(2):e3000128.
33. Therkildsen NO, et al. (2019) Contrasting genomic shifts underlie parallel phenotypic evolution in response to fishing. *Science* 365(6452):487–490.
34. Bergland AO, Behrman EL, O'Brien KR, Schmidt PS, Petrov DA (2014) Genomic evidence of rapid and stable adaptive oscillations over seasonal time scales in drosophila. *PLoS Genet.* 10(11):e1004775.
35. Machado HE, et al. (2018) Broad geographic sampling reveals predictable and pervasive seasonal adaptation in drosophila.
36. Buffalo V, Coop G (2019) The linked selection signature of rapid adaptation in temporal genomic data. *Genetics* 213(3):1007–1045.
37. Kelly JK, Hughes KA (2019) Pervasive linked selection and Intermediate-Frequency alleles are implicated in an Evolve-and-Resequencing experiment of drosophila simulans. *Genetics* 211(3):943–961.
38. Castro JP, et al. (2019) An integrative genomic analysis of the longshanks selection experiment for longer limbs in mice. *Elife* 8.
39. Marchini M, et al. (2014) Impacts of genetic correlation on the independent evolution of body mass and skeletal size in mammals. *BMC Evol. Biol.* 14:258.
40. Robertson A (1961) Inbreeding in artificial selection programmes. *Genet. Res.* 2(2):189–194.
41. Santiago E, Caballero A (1995) Effective size of populations under selection. *Genetics* 139(2):1013–1030.
42. Hayward LK, Sella G (2019) Polygenic adaptation after a sudden change in environment.
43. Nuzhdin SV, Turner TL (2013) Promises and limitations of hitchhiking mapping. *Curr. Opin. Genet. Dev.* 23(6):694–699.
44. Baldwin-Brown JG, Long AD, Thornton KR (2014) The power to detect quantitative trait loci using resequenced, experimentally evolved populations of diploid, sexual organisms. *Mol. Biol. Evol.* 31(4):1040–1055.
45. Santiago E, Caballero A (1998) Effective size and polymorphism of linked neutral loci in populations under directional selection. *Genetics* 149(4):2105–2117.
46. Wray NR, Thompson R (1990) Prediction of rates of inbreeding in selected populations. *Genet. Res.* 55(1):41–54.
47. Woolliams JA, Wray NR, Thompson R (1993) Prediction of long-term contributions and inbreeding in populations undergoing mass selection. *Genet. Res.* 62(3):231–242.
48. Signor SA, New FN, Nuzhdin S (2018) A large panel of drosophila simulans reveals an abundance of common variants. *Genome Biol. Evol.* 10(1):189–206.
49. Howie JM, Mazzucco R, Taus T, Nolte V, Schlötterer C (2018) DNA motifs are not general predictors of recombination in two drosophila sister species.
50. Hendry AP, Kinnison MT (1999) Perspective: The pace of modern life: Measuring rates of contemporary microevolution. *Evolution* 53(6):1637–1653.
51. Hairston, Jr NG, Ellner SP, Geber MA, Yoshida T, Fox JA (2005) Rapid evolution and the convergence of ecological and evolutionary time. *Ecol. Lett.* 8(10):1114–1127.
52. Corbett-Detig RB, Hartl DL, Sackton TB (2015) Natural selection constrains neutral diversity across a wide range of species. *PLoS Biol.* 13(4):e1002112.
53. Coop G (2016) Does linked selection explain the narrow range of genetic diversity across species?, (Cold Spring Harbor Labs Journals), Technical report.
54. Comeron JM (2014) Background selection as baseline for nucleotide variation across the drosophila genome. *PLoS Genet.* 10(6):e1004434.
55. Haller BC, Messer PW (2019) SLiM 3: Forward genetic simulations beyond the Wright-Fisher model. *Mol. Biol. Evol.* 36(3):632–637.
56. Rossum G (1995) Python reference manual, (NLD), Technical report.
57. Oliphant TE (2006) *A guide to NumPy*. (Trelgol Publishing USA) Vol. 1.
58. Kluyver, Thomas Ragan-Kelley, Benjamin Pérez, Fernando Granger, Brian Bussonnier, Matthias Frederic, Jonathan Kelley, Kyle Hamrick, Jessica Grout, Jason Corlay, Sylvain Ivanov, Paul Avila, Damián, Abdalla Safia, Willing Carol and Jupyter development team (2016) Jupyter notebooks-a publishing format for reproducible computational workflows.
59. Hunter JD (2007) Matplotlib: A 2D graphics environment. *Computing in Science Engineering* 9(3):90–95.